Progress in fabrication of waveguide spatial light modulators via femtosecond laser micromachining

Citation: Savidis, Nickolaos, et al. "Progress in Fabrication of Waveguide Spatial Light Modulators via Femtosecond Laser Micromachining." Proceedings Volume 10115, Advanced Fabrication Technologies for Micro/Nano Optics and Photonics X, 28 January - February 2, 2017, San Francisco, California, edited by Georg von Freymann et al., 2017, SPIE, p. 101150R. © 2017 SPIE

As Published: http://dx.doi.org/10.1117/12.2250596

Publisher: SPIE

Persistent URL: http://hdl.handle.net/1721.1/115386

Version: Final published version: final published article, as it appeared in a journal, conference proceedings, or other formally published context

PROCEEDINGS OF SPIE

SPIEDigitalLibrary.org/conference-proceedings-of-spie

Progress in fabrication of waveguide spatial light modulators via femtosecond laser micromachining

Nickolaos Savidis, Sundeep Jolly, Bianca Datta, Michael Moebius, Thrasyvoulos Karydis, et al.

Nickolaos Savidis, Sundeep Jolly, Bianca Datta, Michael Moebius, Thrasyvoulos Karydis, Eric Mazur, Neil Gershenfeld, V. Michael Bove, "Progress in fabrication of waveguide spatial light modulators via femtosecond laser micromachining," Proc. SPIE 10115, Advanced Fabrication Technologies for Micro/Nano Optics and Photonics X, 101150R (20 February 2017); doi: 10.1117/12.2250596

SPIE.

Event: SPIE OPTO, 2017, San Francisco, California, United States

Progress in fabrication of waveguide spatial light modulators via femtosecond laser micromachining

Nickolaos Savidis[a], Sundeep Jolly[a], Bianca Datta[a], Michael Moebius[b], Thrasyvoulos Karydis[c], Eric Mazur[b], Neil Gershenfeld[c], and V. Michael Bove, Jr.[a]

[a]MIT Media Lab, Massachusetts Institute of Technology, Cambridge, MA, United States
[b]School of Engineering and Applied Sciences, Harvard University, Cambridge, MA, United States
[c]Center for Bits and Atoms, Massachusetts Institute of Technology, Cambridge, MA, United States

ABSTRACT

We have previously introduced a femtosecond laser micromachining-based scheme for the fabrication of anisotropic waveguides in lithium niobate for use in a guided-wave acousto-optic spatial light modulator. This spatial light modulation scheme is extensible to off-plane waveguide holography via the integration of a Bragg reflection grating. In this paper, we present femtosecond laser-based direct-write approaches for the fabrication of (1) waveguide in-coupling gratings and (2) volume Bragg reflection gratings via permanent refractive index changes within the lithium niobate substrate. In combination with metal surface-acoustic-wave transducers, these direct-write approaches allow for complete fabrication of a functional spatial light modulator via femtosecond laser direct writing.

Keywords: guided-wave acousto-optics, femtosecond laser micromachining, laser-written waveguides, laser-written gratings, lithium niobate, volume gratings

1. INTRODUCTION

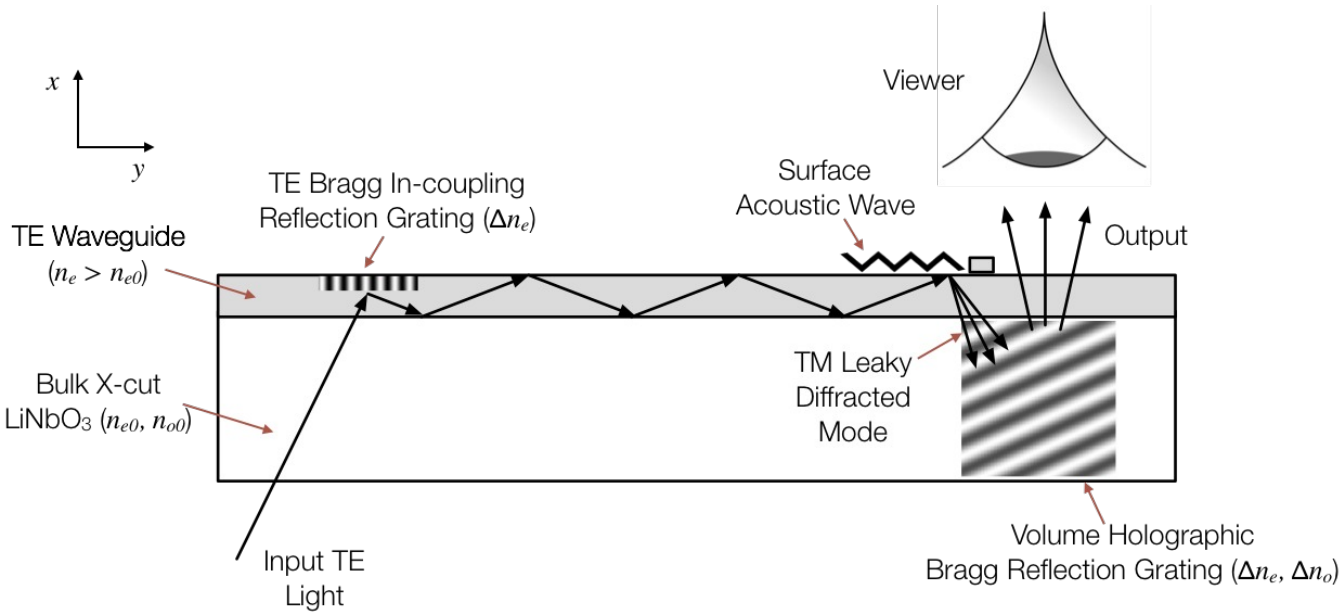

Figure 1: $x - y$ cross-section (side view) of proposed guided optical wave SAW device with integrated Bragg gratings.

A holographic video display based on space-multiplexed, guided-wave acousto-optic spatial light modulation capable of transparent or opaque viewing operation is realizable.[1] There are three base elements that comprise the piezoelectric

Corresponding author: nsavidis@media.mit.edu

Advanced Fabrication Technologies for Micro/Nano Optics and Photonics X, edited by Georg von Freymann, Winston V. Schoenfeld, Raymond C. Rumpf, Proc. of SPIE Vol. 10115, 101150R
 · doi: 10.1117/12.2250596

lithium niobate acousto-optic modulator: 1) the anisotropic waveguide, 2) the surface acoustic wave (SAW) transducer, and 3) the input / output coupler (see Figure 1). Waveguide fabrication for these and similar SAW devices currently relies on proton exchange of a lithium niobate substrate within the modulator process, which involves the immersion of the substrate in an acid melt.[1,2] While simple and effective, waveguide depth and index profiles resulting from proton exchange are often non-uniform over the device length or inconsistent between waveguides fabricated at different times using the same melt and annealing parameters. In contrast to proton exchange, direct writing of waveguides has the appeal of simplifying fabrication (as these methods are inherently maskless) and the potential of fine and consistent control over waveguide depth and index profiles.[3,4]

We explore femtosecond laser micromachining as an alternative to proton exchange in the fabrication of waveguides for anisotropic leaky-mode modulators. Femtosecond laser micromachining offers a platform where all three base elements of the acousto-optic modulator can be embedded into the lithium niobate.[4] In this paper we focus on the creation of holographic volume gratings as in-coupling / out-coupling elements. In addition, we create anisotropic waveguides by altering the refractive index within the lithium niobate to create a core / cladding structure that is traditionally observed in optical waveguides.[5,6]

2. FEMTOSECOND LASER MICROMACHINING

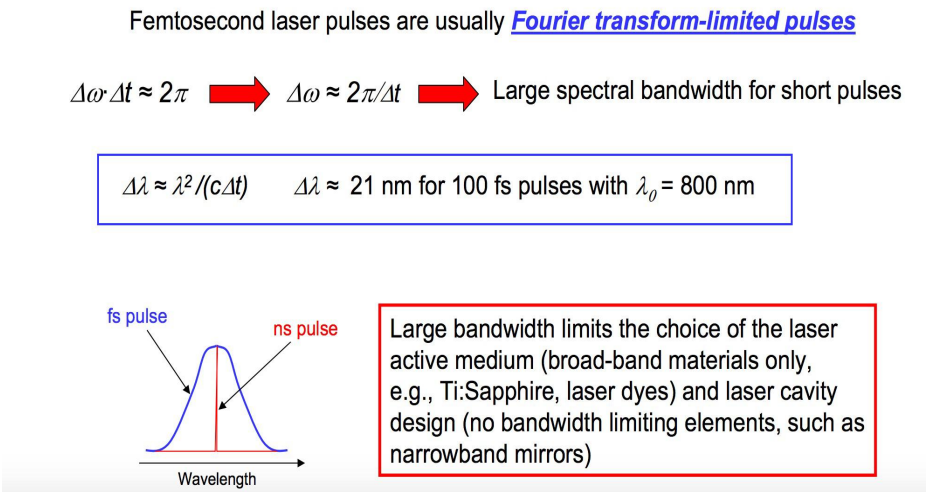

Figure 2: Femtosecond pulses are formed by generating a long frequency bandwidth.

Recent advancements in femtosecond lasers, tunable in the ultra-violet, visible and near- infrared spectral regions, offer tremendous possibilities in machining and altering the properties of materials with feature sizes in the μm regime. Femtosecond laser pulses are usually Fourier transform-limited pulses- they are formed due to simultaneously oscillating modes from a broad frequency bandwidth. The most common technique to achieve femtosecond pulsed lasing is Kerr lens modelocking. A typical setup includes a pump laser and an optical medium which facilitates the Kerr effect (i.e., nonlinear refractive index), depending on the intensity of the light.

A pulse that builds up in a laser cavity containing a gain medium and a Kerr medium experiences not only self-phase modulation but also self-focusing, which entails nonlinear lensing of the laser beam due to the nonlinear susceptibility of the Kerr medium. A spatiotemporal laser pulse propagating through the Kerr medium has a time dependent mode size as higher intensities acquire stronger focusing. If a hard aperture is placed at the right position in the cavity, it strips off of the ends of the pulse, leading to a shortening of the pulse. Femtosecond pulses with energy of several nJ result in mW peak intensities due to their short duration. Such intensities, when tightly focused can produce electric fields which enable photo-ionization, plasma generation, and atomic bond breaking in the targeted material as generated fields surpass the energy gap of the valence electrons.

There are five primary parameters that affect the resolution and thus the accuracy of our point ionization.[7] These parameters are: 1) The spot size due to the NA of the objective lens, 2) the light intensity, 3) the exposure time / repetition rate, 4) the

wavelength of the femtosecond pulses, and 5) material selection. Here we present a system that controls all five of these primary parameters.

3. METHODOLOGY: INSTRUMENTATION FOR WAVEGUIDES AND VOLUME BRAGG GRATINGS

There are two primary instruments and an objective that enable us to control the first four of the five parameters, which inherently control the point ionization. We apply a Pharos DPSS Femtosecond Laser as our light source and the Aerotech nano positioning stage as our activation location control. The Pharos femtosecond laser offers built in controls for light intensity, repetition rate, and the operating wavelength. The Aerotech stage controls the positioning and the exposure time of the position when coupled to the repetition rate.

The 25W Pharos is selected as this power can be distributed across a wide range of materials and serves for a broad range of experimental purposes. In addition, there is a built-in Pockels cell and amplifier to control the intensity output and repetition rate. The power can therefore be reduced to exposures of nanojoules (nJ) per pulse. The experimental system also applies a polarizer and half waveplate to further control the light polarization and intensity of the outputted light. The Pockels cell is built in the Pharos to control the repetition rate of the laser pulse. The system varies the repetition rate from the MHz range to low kHz rates using the pulse picker. The repetition rate is controlled in discrete integer values, where single shot exposure is achievable. The pulse duration of the Pharos is below 290 nm under all conditions, offering a controlled output.

A further control of the spot size is offered by the wavelength selection. The fundamental wavelength operates at 1030 nm, but a harmonic generator can be applied to lower to fixed wavelength. We applied the second harmonic, which operates at 515 nm in order to visualize our optical beam. In the future we will apply the higher harmonics (which the Pharos offers to the fifth harmonic) in order to decrease the spot size.

The second primary component is a custom-made Aerotech nano-positioning stage. There is a combination of three nanopositioning stages that are oriented in x, y, z directions. The stage is placed on a granite base and a floating optical bench in order to eliminate vibrations from both the room and the stage positioners. The high performance air bearing stages offer 1 nm resolution, 75 nm repeatability and 250 nm accuracy. This is significant in that it allows for spot size features to have the size of 250 nm without eliminating the possibility of continuity. Features as small as 250 nm can be produced with optimized objectives and optics. These single spots are combined when the stage is moved to produce lines for waveguides or volume gratings. The movement of the stages operate at a speed of 100 mm / sec. The speed of the stage is significant as stage speed is a mechanism to control the exposure time per area. This speed, the repetition rate of the Pharos laser, and the selected intensity of the exposure time are the key variables for this setup.

The combination of the femtosecond laser with the nanopositioning stages offers the control necessary to experiment with the majority of the parameters that alter the outcome of the micromachining process. The final two parameters are the material and the proper objective. Lithium niobate is selected as the acousto-optic modulator target due to its piezoelectric properties.

The final selection parameter is the objective, where the light entering the objective is collimated from infinity. The only restriction defined by the proposed setup is that the objective spot size is larger than the 250 nm defined by the accuracy of the stage positioning. The aim is to apply the objective with the highest NA (and thus the smallest spot size) for the volume Bragg gratings without reaching below this positioning limitation. We applied the 3.5 mm working distance 0.8 NA 100X Nikon Planar field corrected objective, which both the waveguide and the volume Bragg gratings use as it offered a lower limit on the size of waveguides and feature sizes.

4. METHODOLOGY: FABRICATION AND EXPERIMENTATION FOR WAVEGUIDES AND VOLUME BRAGG GRATINGS

Fabrication of the waveguides and gratings requires the same functional setup. The orientation of the writing process is vertical. In order to achieve this orientation, the propagating beam must enter above the objective. The Pharos laser outputs a beam, which is expanded by 2.5x to fill the back aperture of the objective. The light enters a periscope that is parallel to the optical bench, but is raised by a meter.

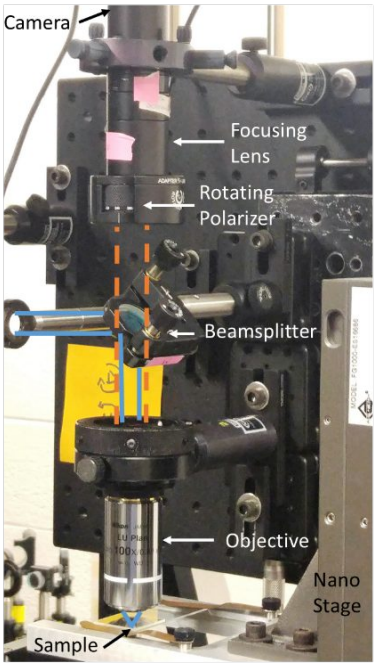

Figure 3: A combination of writing and imaging at the objective region. The collimated light entering the setup is drawn in blue (solid) and enters through an aperture stop. Additionally, the dashed orange line illustrates the collimated light leaving the sample and entering the polarizer for the camera. The camera is applied to verify image writing location while the stage is adjusted for proper pattern writing through the objective.

The collimated light reaches the objective region as is observed in Figure 3. With the light expanded, the aperture stop is adjusted to match the aperture size of the objective. This reduces the scatter at the objective. The light then propagates to a beamsplitter, which is designed at a transmission of 92% of the light with 8% reflection. The majority of the light propagates through to the objective. It is necessary to measure the pulse energy at the sample as it is reduced relative to the source. The objective then focuses the light onto the sample. A camera is used to image the location on the sample. The z location on the stages is adjusted until a clear image is observed on the camera. When the sample is clear on the camera, we are focused at the write location on the objective. The position and exposure time of the laser is then controlled by the x,y,z nano positioning stages.

4.1 Waveguides

The waveguides produced within the lithium niobate are achieved by controlling parameters of the femtosecond laser, the positioning stages, and an additional half wave / polarizer. Table 1 illustrates the parameter variation that enabled the writing of the waveguides. Fourteen separate waveguide rows are written. Each pattern row contains five sets of five waveguides, with a total of 350 waveguides produced.

There are three parameters that are altered in order to produce variation in the waveguide quality. The majority of the laser settings are fixed. The target change in power varied from 100 nJ to 400 nJ, in increments of 50 nJ. The power is achieved by keeping the polarizer fixed in the writing path, the femtosecond laser fixed at an output of 10%, and the half wave plate rotated in order to control the output power. At each fixed power there are 10 sets of waveguides written, with every two rows offered the same output power. The change in each set per row is due to the rate at which the micromachining stage shifts. The stage speed can be decreased from 2000 μm / sec to 10,000 μm / sec in 2000 μm steps. Therefore, each row offers five separate writing speeds for each intensity.

The first, third, and fifth waveguide within each set are written with the stage shifting from the top down. The second and fourth waveguides are written from the bottom up. These experiments are used to determine if the stage travel orientation alters the waveguide exposure.

Pattern Row	Rep Rate (kHz)	Pulse Duration (ns)	Polarizer Setting (Deg)	Laser Transmission (%)	Power after Polarizer (W)	Pulse Energy @ Sample (μJ)	Velocity μm/s			Shot
							Max	Step	Min	
1	50	230	360	10	0.043	0.1	10000	2000	2000	Single
2	50	230	360	10	0.043	0.1	10000	2000	2000	Half
3	50	230	360	10	0.064	0.15	10000	2000	2000	Single
4	50	230	360	10	0.064	0.15	10000	2000	2000	Half
5	50	230	360	10	0.085	0.2	10000	2000	2000	Single
6	50	230	360	10	0.085	0.2	10000	2000	2000	Half
7	50	230	360	10	0.106	0.25	10000	2000	2000	Single
8	50	230	360	10	0.106	0.25	10000	2000	2000	Half
9	50	230	360	10	0.128	0.3	10000	2000	2000	Single
10	50	230	360	10	0.128	0.3	10000	2000	2000	Half
11	50	230	360	10	0.15	0.35	10000	2000	2000	Single
12	50	230	360	10	0.15	0.35	10000	2000	2000	Half
13	50	230	360	10	0.171	0.4	10000	2000	2000	Single
14	50	230	360	10	0.171	0.4	10000	2000	2000	Half

Table 1. The parameters altered for the 350 waveguides. The primary parameter changes are the pulse energy at the sample, the speed of the nanostage, and the shot trigger to output the pulse.

Two rows are written with each intensity as the triggering is set between a half and a single shot. There is a scripting interface written in G code that enables the writer to control the trigger for the laser and the stage speeds. The script allows for the application of a single shot for each location. Alternatively, the laser can be programmed to release a shot for every other move. Altering this parameter offers a control for reducing the exposure time without reducing the speed of the stage. Theoretically, this would enable smoother writing between adjacent points.

4.2 Volume Bragg Gratings

The volume gratings are written with the same optical setup as the waveguides using alternative beam parameters. The trigger speed, stage speed, and intensity are fixed to reduce variability of each point. For initial experiments, the testing of the volume gratings is performed on a borosilicate glass slide rather than lithium niobate in order to avoid nonlinear or anisotropic refractive index effects.[8–10]

Table 2 and Figure 4 illustrate the experimental parameters used to determine the impact of layer design within the volume grating. There is a total of 25 grating patches in which clusters are written with specific z-spacing. The gratings are written with x, y resolution of 2 μm and a pulse energy of 150 nJ. In addition, each grouping began with a single grating layer and each test grating area systematically included an additional layer.

The first patch grouping 1-4 (shown in Figure 4) is a series of gratings containing between a single layer to four layers. The number of layers increases per patch within a grouping. Therefore, the second patch has two grating layers separated by eight μm. The third patch has three grating layers separated by eight microns each. Similarly, patch 11 is a single grating layer while patch 12 is two grating layers with a 15 μm separation. Patch 17, the final patch within that grouping, has a total of seven written grating layers with 15 μm separation.

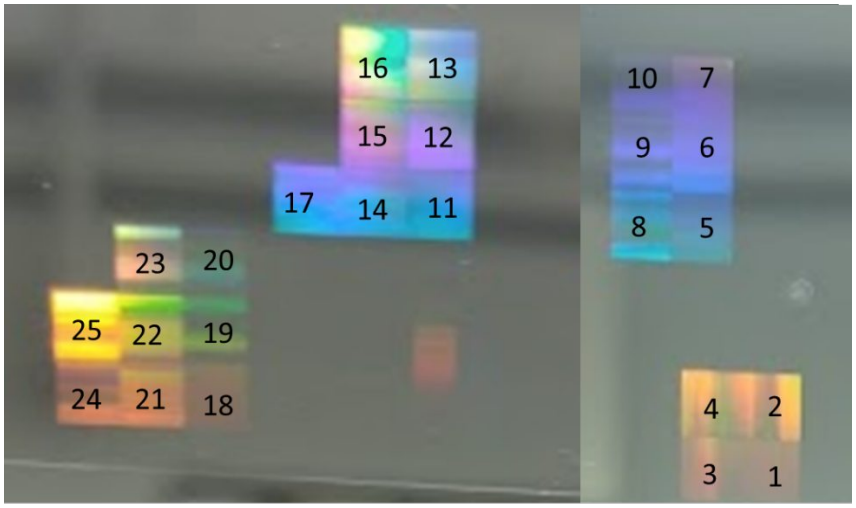

Figure 4: The output of 25 different gratings where the first of each set is a single layer and the layers increase as the number value increases. The spacing in each set is altered between layers. Sets 1-4 have 8 μm layer separation, 5-10 have 10 μm layer separation, 11-17 have 15 μm separation and 18-25 have 20 μm separation.

Patch	X Resolution (μm)	Y Resolution (μm)	Z Layer Spacing (μm)	Grating Layers	Pulse Energy @ Sample (nJ)	Patch	X Resolution (μm)	Y Resolution (μm)	Z Layer Spacing (μm)	Grating Layers	Pulse Energy @ Sample (nJ)
1	2	2	8	1	150	13	2	2	15	3	150
2	2	2	8	2	150	14	2	2	15	4	150
3	2	2	8	3	150	15	2	2	15	5	150
4	2	2	8	4	150	16	2	2	15	6	150
5	2	2	10	1	150	17	2	2	15	7	150
6	2	2	10	2	150	18	2	2	20	1	150
7	2	2	10	3	150	19	2	2	20	2	150
8	2	2	10	4	150	20	2	2	20	3	150
9	2	2	10	5	150	21	2	2	20	4	150
10	2	2	10	6	150	22	2	2	20	5	150
11	2	2	15	1	150	23	2	2	20	6	150
12	2	2	15	2	150	24	2	2	20	7	150
						25	2	2	20	8	150

Table 2. The parameters that are altered for the 25 patches are the grating layers and the grating spacing.

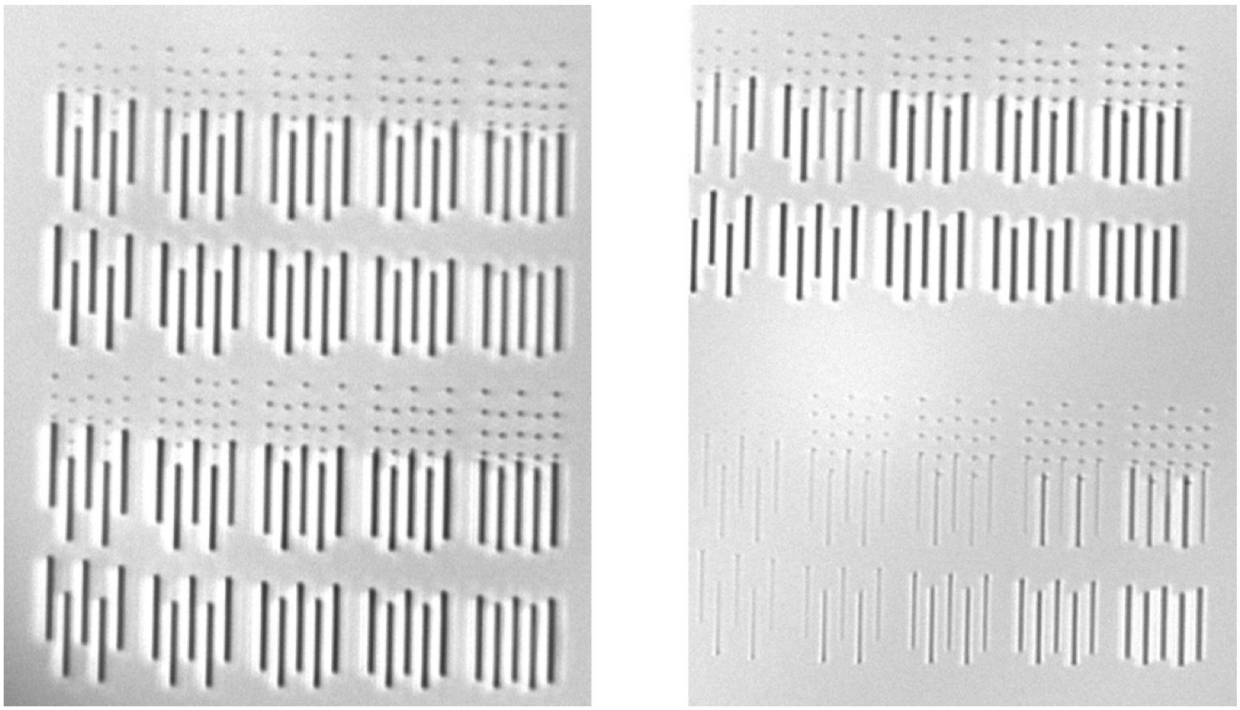

Figure 5: Wide field of view image of the waveguides in a series pattern.

5. RESULTS: WAVEGUIDE PARAMETERS

The variation of three parameters for the waveguides outputted a total of 350 waveguides. Figure 5 is an image of eight out of the fourteen waveguide layers. In addition to the waveguides, we wrote sets of points to observe the quality of each outputted spot. As is observed from Figure 5, the bottom right image illustrates waveguides that are written below a threshold that would enable solid waveguide outputs. At the lower pulse energy, slower write speeds are observed to bring the waveguide pattern above threshold. Also, as the speed of the stage is decreased, the exposure time is increased and thus the intensity per area is increased. It is also observed that as we slow the stage speed down, the waveguide positions are controlled. Positioning is shifted by the direction of the writing as is observed in the top left corner of Figure 5.

There are six primary conditions that describe the 350 waveguides as is observed in Figure 6. When the intensity of the exposed area is too low the waveguides do not fully develop within the lithium niobate as is observed in Figure 6a. Increased intensity is required for densification to occur. It is observed that the writing speed and intensity are decreased per pattern row. Alternatively, the trigger speed is decreased as is seen in the difference between row 1 and row 2, allowing for increase of exposure per area.

These parameters resulted in the patterns seen in Figure 6b, where certain waveguides reached threshold while others did not. Figure 6b illustrates that waveguides 2 and 4 reached densification while waveguides 1, 3, and 5 did not. Waveguides are written along the z axis of the crystal. However, waveguides 2 and 4 are written at a direction of 180° relative to the write of waveguides 1, 3, and 5. This suggests that even along the same crystalline axis there is a change in power exposure relative to the direction of the write.

Once all waveguides reach threshold it appears that this directional limitation disappears. The waveguides shown in Figure 6c. are continuous and stable. Under this third condition, the width between the waveguides is the most stable and exhibits the smallest standard deviation in width size. As the intensity of the input beam increases, the size of the waveguide increases (as is observed in Figures 6d and 6e). Figure 6d shows stable waveguides with slower writing speeds vs. Figure 6e which shows waveguides with faster writing speed. Positioning error increases, which can be corrected with a positioning algorithm.

The final condition that characterizes a set of waveguides is when the material is overexposed. This occurs when the input beam power is too high, the stage speed is too low, or the trigger is a full shot rather than half a shot. As is observed in

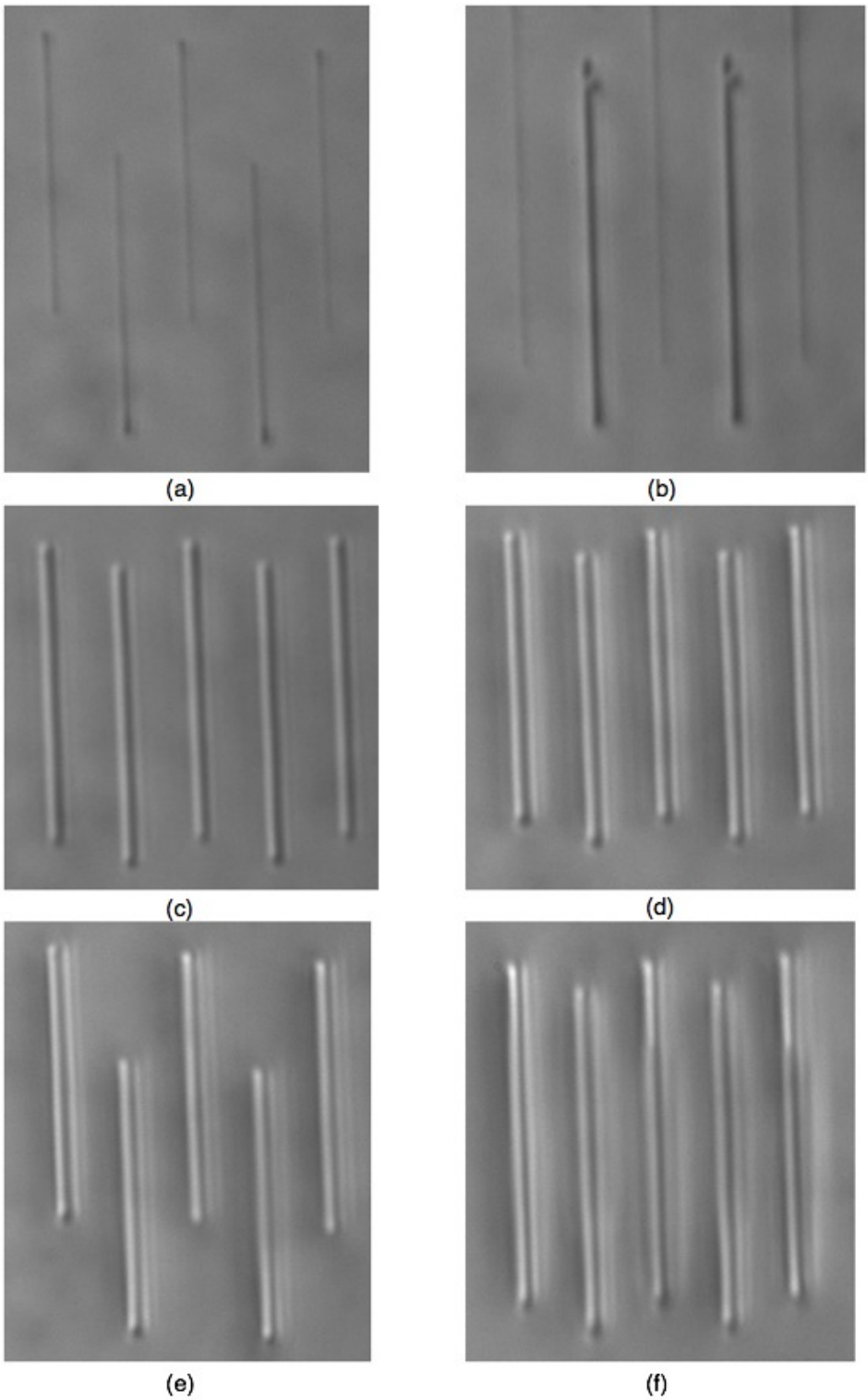

Figure 6: The six primary conditions observed from the 350 waveguides outputted. (a) is waveguides below threshold, (b) a couple of waveguides above threshold, (c) waveguides slightly above threshold, (d) waveguides above threshold with slower writing rates, (e) waveguides above threshold with fast writing rates, and (f) over exposed waveguides.

Figure 6f, the waveguide does not appear continuous. Bulging occurs towards the middle with a darker color relative to the shine sides. These waveguides are no longer continuous and thus are defined as our upper limit in the range of writeable waveguides.

Beyond the six conditions, the waveguides were measured with two approaches. The width of the waveguides is measured with the stage steps. The stage offers incremental repeatability of 50 nm and accuracy of 250 nm. We stepped across each waveguide by a sum of 0.25 μm, or the stage accuracy, and measured the width of each individual waveguide twice. In addition, since the sets are groups of five waveguides, we further averaged those waveguides out to develop an average width for a given row and a given set.

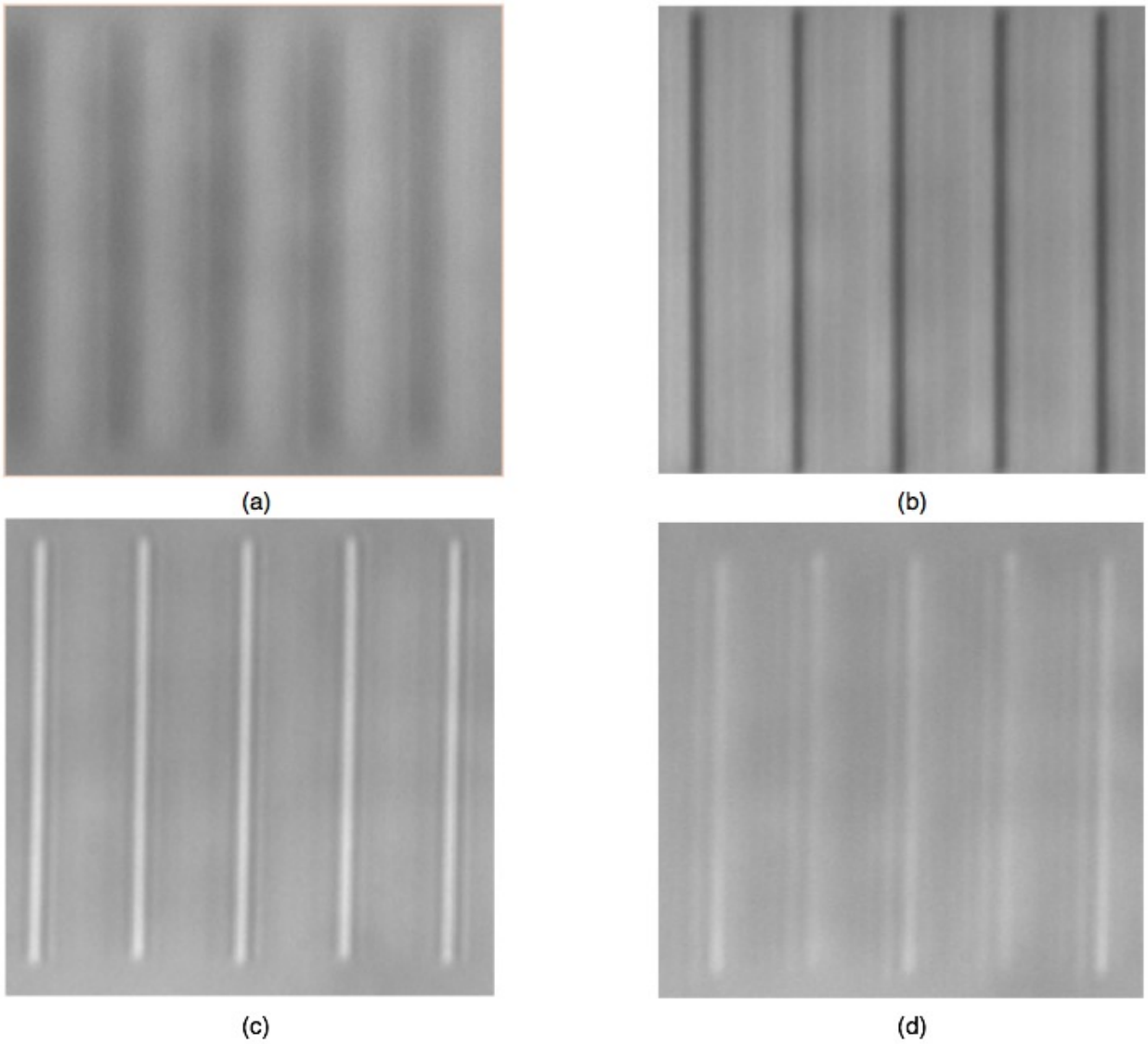

Figure 7: When imaging through focus of the waveguides, one is able to observe four distinct aspects of the waveguide. The separation of the two clear contrast images enables one to measure variation in depth of the image.

The depth of the waveguides is measured in addition to the width of the waveguides. The depth is the imaged depth rather than the actual physical depth as the refractive index of the material is not unity. We are, however, able to determine the variation in depth as is observed within the waveguide by shifting axially through focus along the z-axis. Figure 7 illustrates this through focus of a single waveguide set. The first series of shells is observed when the waveguide is located below the focus of the imaging device. There are two clear image locations that are observed in Figure 7b. and 7c. As the

stage is incrementally shifted axially, there is an outer shell that is observed such as that of Figure 7d. The separation in z distance is measurable between two contrast images of Figures 7b. and 7c. The change in contrast offers details in the depth variation that is measured.

Row	Set	Average width (μm)	Width Std (μm)	Waveguide Depth (μm)	Threshold Difference (μm)	Row	Set	Average width (μm)	Width Std (μm)	Waveguide Depth (μm)	Row	Set	Average width (μm)	Width Std (μm)	Waveguide Depth (μm)
1	1	1.10	0.14	17.73	Below	6	1	3.14	0.09	27.62	11	1	3.80	0.11	45.00
1	2	1.20	0.11	16.25	Below	6	2	3.18	0.10	25.70	11	2	3.74	0.18	42.00
1	3	1.35	0.14	13.50	Below	6	3	3.33	0.05	19.36	11	3	3.57	0.10	38.75
1	4	1.90	0.68	12.75	16.25	6	4	3.43	0.05	19.72	11	4	3.35	0.06	34.75
1	5	2.80	0.51	12.50	Above	6	5	3.57	0.06	16.00	11	5	3.03	0.06	32.01
2	1	1.20	0.14	12.51	Below	7	1	2.54	0.08	27.00	12	1	3.55	0.13	43.00
2	2	1.55	0.41	12.25	15.63	7	2	2.98	0.06	25.25	12	2	3.35	0.10	39.00
2	3	2.28	0.14	10.67	Above	7	3	3.13	0.13	22.75	12	3	3.23	0.14	36.50
2	4	3.03	0.06	7.25	Above	7	4	3.45	0.21	22.01	12	4	2.88	0.18	35.75
2	5	3.75	0.00	5.50	Above	7	5	3.45	0.21	21.01	12	5	2.83	0.11	33.00
3	1	2.25	0.00	31.00		8	1	3.28	0.19	33.25	13	1	1.08	0.07	43.00
3	2	2.28	0.06	29.00		8	2	3.30	0.21	31.90	13	2	1.05	0.07	37.25
3	3	2.70	0.11	24.50	Above	8	3	3.54	0.08	23.22	13	3	1.05	0.07	35.25
3	4	3.00	0.00	19.00		8	4	3.61	0.10	23.94	13	4	0.95	0.07	31.72
3	5	3.15	0.14	19.99		8	5	3.74	0.03	21.00	13	5	0.90	0.10	27.75
4	1	3.00	0.00	22.00		9	1	3.88	0.18	39.46	14	1	0.90	0.06	25.50
4	2	3.05	0.07	19.50		9	2	3.85	0.14	38.25	14	2	0.80	0.07	22.75
4	3	3.13	0.13	15.50	Above	9	3	3.70	0.11	38.20	14	3	0.78	0.06	22.50
4	4	3.25	0.00	15.50		9	4	3.70	0.11	34.25	14	4	0.78	0.06	15.25
4	5	3.40	0.14	10.99		9	5	3.73	0.14	32.75	14	5	0.75	0.00	12.00
5	1	2.43	0.07	29.00		10	1	3.75	0.18	36.50					
5	2	2.60	0.06	27.13		10	2	3.60	0.14	33.99					
5	3	2.91	0.10	23.63	Above	10	3	3.65	0.16	27.00					
5	4	3.23	0.10	20.52		10	4	3.50	0.00	24.75					
5	5	3.30	0.11	16.48		10	5	3.25	0.09	22.74					

Table 3. Testing results for the 350 waveguides that are produced across the parameter sweep of intensities, exposure rates, and trigger speeds.

There is a significant difference between the width of the waveguides produced under the six conditions. When the waveguides are under threshold, the measured width is near the 1 μm range as is observed in the results in Table 3. Once threshold is reached, the width shifts to 2 μm. The various settings after threshold alters the width of the waveguides to between 2.25 to 3.9 μm in width. The standard deviation for the width is narrower for the waveguides that are closer to the lower energy threshold. As intensity increases, the waveguides begin to increase in standard deviation. In addition, the waveguides begin to diminish in width once the waveguides are completely over-exposed as is observed in rows 13 and 14.

The waveguides demonstrate a linear change in width as the writing speed per lane is adjusted. The width increases as the stage speed is reduced for rows 1-8. There is an inversion at row 9 which suggests that the increase in intensity accelerates the point exposure, and the width begins to decrease. This pattern in width reduction continues as we progress through rows 9-14. The majority of the settings for rows 1, 2, 13, and 14 are in conditions where the waveguides do not perform uniformly. The one exception is row 2 set 5, where the waveguides are not only uniform, but exhibit zero standard deviation. This data suggests that waveguides are achievable in lithium niobate with pulse energies of 150 nJ-350 nJ when

the stage operates at speeds of 2,000 μm / sec to 10,000 μm/ sec. In addition, within these laser intensities and stage operating speeds, the trigger synced with the software can operate at single or half a shot.

The distinction between the clear image and full bright contrast image also offers depth information for the rows and sets. The depth demonstrates the same trend as width, as we decrease the stage rate we observe that for rows 1-14, the depth decreases. Again these are not absolute depths, but relative depths through the imaging medium. There is a subtle change between rows 1-8 and rows 9-14. In rows 1-8, the single shot begins at a higher separation value than the double shot. For example, row 1 set 1 begins at 17.73 μm vs. row 2 set 1 that begins at 12.51 μm. This trend continues for the first eight rows but inverses for sets 8-14. This depth variation coupled with the change in width trends illustrates a functional change within the lithium niobate during direct writing.

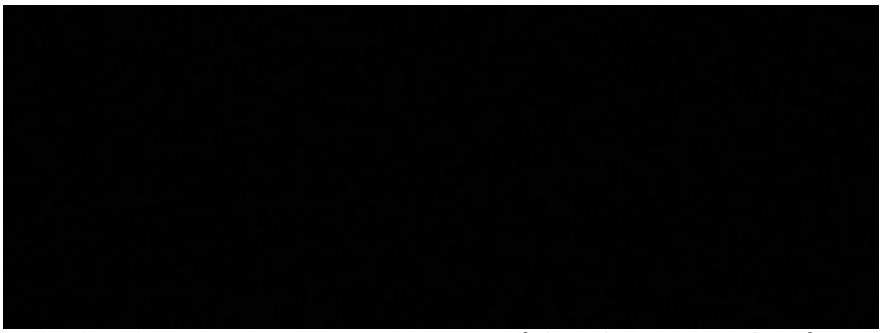

Figure 8: The waveguide is written to rotate the waveguides by 15° for a full rotation of 180° to observe the effects on relative depth imaging.

There are additional changes observed relative to depth variation and writing orientation. The orientation of the writing process is found to alter the threshold as is observed in row 2 measurements. In addition, the writing is not limited purely along a single axis. The lithium niobate is x-cut and thus writing orientation is on the y and z axis. Figure 8 shows our set of waveguides rotated by 15° for a full rotation of 180°. The measurement of the depth thickness showed that as the stage is rotated about the writing direction, the waveguide depth measurement changed. The waveguide depth decreased from 0° to 90°, but then increased from 90° to 180°. There is symmetry relative to the 90° with a similar plateau and shape as seen in Figure 9. The change in relative thicknesses for all of the waveguides is produced by either one of two possibilities: 1) The physical thickness of the waveguide is increasing relative to exposure or 2) the refractive index is being controlled relative to the parameter sweep. A further investigation is required to determine the which effects contribute most directly to the observed results.

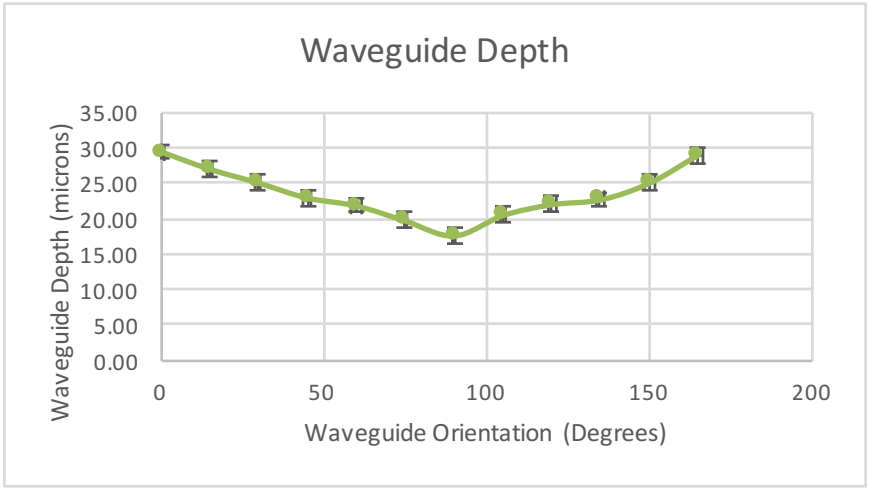

Figure 9: The writing orientation into the waveguide plays a significant role in the observed thickness of the waveguide.

6. RESULTS: VOLUME BRAGG GRATINGS

As described above, the target for the volume gratings experiments is to determine the axial spacing between grating layers in order to achieve distinguished grating layers. As the femtosecond laser writing is orthogonal to the surface, the energy is entering along the z axis. The axial resolution is dependent on the axial absorption, which is defined by the photo-ionization energy threshold to produce densification. Transversely, there is tight confinement within the spot, allowing for control. Longitudinally, however, the confinement is dependent on the objective: numerical aperture, the avalanching threshold, the repetition rate and intensity of the source, the stage positioning, and other parameters that effect exposure time.

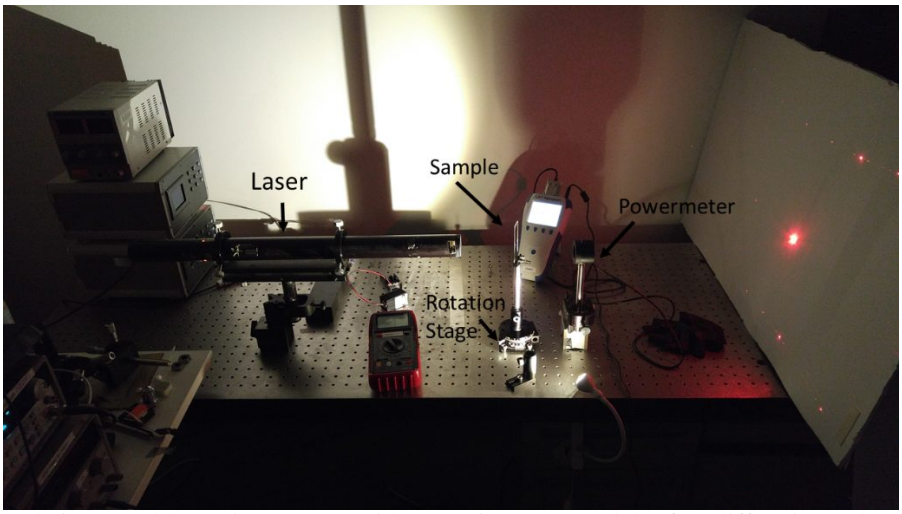

Figure 10: The sample is rotated by 1° increments with a rotation stage and the first diffractive ordered is measured with a powermeter. The samples' angular sensitivity is measured for each volume grating.

Two parameters are adjusted to determine the volume gratings axial spacing quality: 1) the z-spacing between grating layers and 2) the number of layers written. The output of the first order diffraction from a two dimensional grating pattern is measured by the apparatus designed in Figure 10. The light source is aligned to the center of rotation of the rotation stage. This ensures that the light source remains on the grating patch as the stage rotates angularly. The sample is rotated in one degree increments from zero to twenty degrees in order to measure the angular sensitivity of the first diffractive order. A power meter is placed at the first diffractive order propagation location in order to measure the beam intensity.

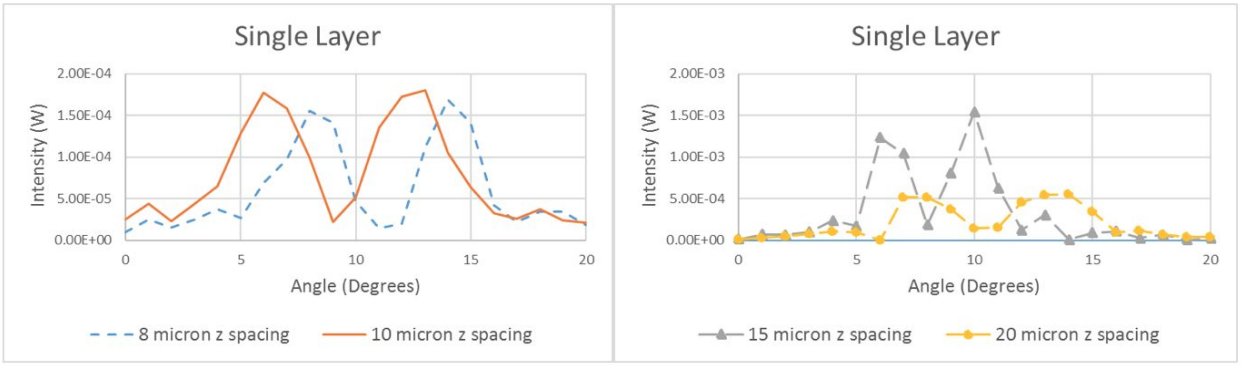

Figure 11: The single layer patches for all four sets output matching pattern shapes with approximately the same peak separations validating a consistent process.

As a first order validation, a single layer is produced for the 8 μm, 10 μm, 15 μm and 20 μm layers. All four of these diffraction gratings should produce the same angular sensitivity as the settings are fixed for all four patches. As is observed in Figure 11, all of four of these single layer diffraction gratings produced two distinct peaks. This suggests that the point by point modifications are producing densification in the x and y dimensions as anticipated. The separation between the two

peaks is 6o for the 8, 10, and 20 μm z spacing sets while the two peak separation is 5° for the 15 μm set. The discrepancy for the 15 μm set may be attributable to the course increments applied to the measurement of the angular sensitivity. The shape and peak separation are approximately equivalent, validating that the process between the groups is consistent.

As testing verified that the four sets have a consistent process, we are able to determine the effects of the z axis separation across the grating layers. Figure 12 shows a combination of grating layers increasing from two grating layers to eight grating layers. The 8 μm, and 10 μm z spacing separation output lower intensity thresholds relative to the 15 μm and 20 μm separation of grating layers. It is highly probable that the closer the grating layers are to each other, the higher the destructive interference. In addition, the volume gratings that operate with 8, 10 and 15 μm separations output similar results to a single layer even when the volume grating is increased to seven layers. This suggests that the volume gratings for 8, 10, and 15 μm separations are not in fact volume gratings but rather singular layer gratings, as the layers have combined to create a single diffraction grating layer.

There is a distinction between the 20 μm separated grating layers of the volume grating and the other separations. When the volume grating with 20 μm separation has three grating layers or fewer, it operates similar to the other gratings. With four to six grating layers in the volume grating, peaks and valleys develop, as would be anticipated by the angular selectivity of a volume grating. After seven grating layers with 20 μm separation, distinct peaks and valleys are observed with a more even spacing. The results suggest that with the currently selected parameters and optics, volume holograms are achievable with seven grating layers or more at a 20 μm separation. These results suggest diffractive behavior consistent with stratified volume holographic elements and indicate that Bragg-like diffraction is achievable with increasing number of layers and tuned inter-layer spacing.[11]

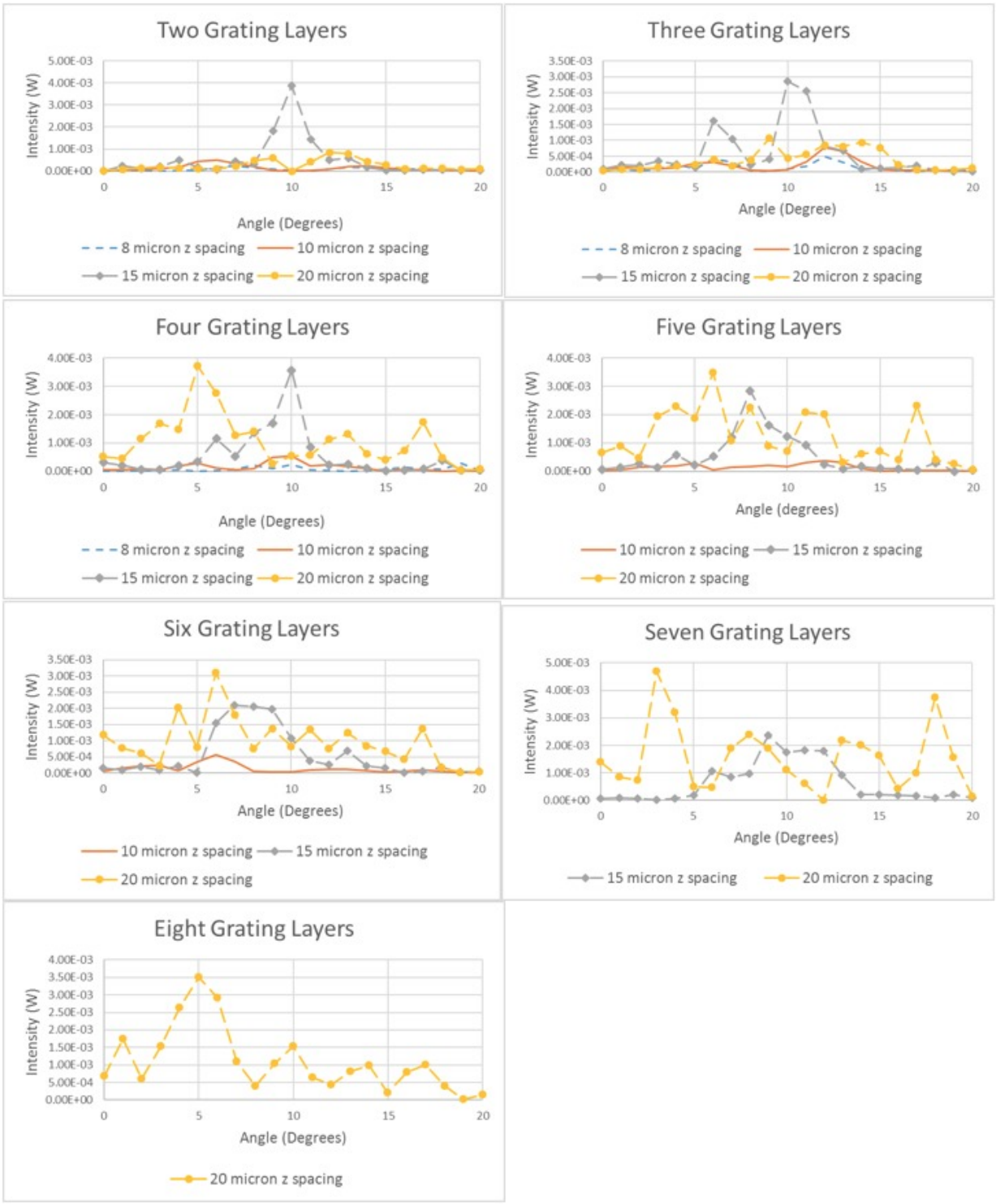

Figure 12: First-order diffracted intensity as a function of beam incidence angle for varying inter-layer spacings and number of layers.

7. FUTURE WORK

Further development is required for both the waveguide writing and volume gratings in order to achieve the goal of direct writing an acousto-optic spatial light modulator. Here we evaluate each writing process separately as they each have different development requirements.

The application of the femtosecond laser for direct writing volume gratings has shown promise. The current setup has proven that we are able to measure angular sensitivity of a volume grating for the first diffractive order. These measured results require refinement as is mentioned in the volume gratings section above. A new approach is required to produce a more accurate measurement of the angular sensitivity of the volume grating.

An additional target after improving the measurement approach is to develop a method to reduce the spacing between grating layers. With the current setup, it is possible to reduce the layers by reducing the intensity of the incoming femtosecond laser while also reducing the speed of the nano stage. Reducing the nano stage speed increases the exposure time, and reducing the intensity decreases the amount of flux per second. The reduction of intensity would reduce the axial exposure along the z axis and thus would theoretically trigger ionization longitudinally along the z axis direction in a confined space. Alternatively, a change in objective would also allow for a decrease in grating spacing. A faster objective would focus the light to a smaller spot and spread the light further axially. This increased focus would require a reduction in energy, also improving the point quality transversely.

A further step is to begin testing grating layers in non-linear optical mediums, such as lithium niobate. These experiments are performed on a linear, homogeneous, isotropic material, borosilicate, in order to reduce the variables. This allowed for a validation of volume grating creation with the application of the femtosecond laser. Ultimately, a shift to lithium niobate is required as the base substrate used for the acousto-optic modulator.

The waveguides are tested on lithium niobate, but also require further experimentation to better characterize the generated waveguides. A cross-sectional analysis of the physical waveguide is required for all of the waveguide settings. This is necessary to determine the change in refractive index of the waveguide. Once the refractive index is known, one is able to determine the properties needed for the volume grating to couple light in and out of the waveguides to the volume gratings.

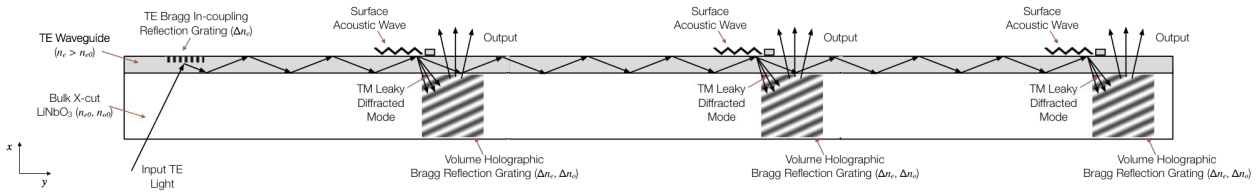

Figure 13: The ultimate goal is to produce a flat-panel element-based (i.e., hogel-based) holographic display in which each element is composed of directly written waveguides, volume gratings, and metal transducers on or in an anisotropic substrate such as lithium niobate.

The ultimate goal is to produce a flat-panel holographic display. The future work is targeted towards the development of a stable process that will enable the output of several acousto-optic modules on the same waveguide to produce a series of hogels or holographic pixels. Figure 1 represents a single acousto-optic element capable of modulating only a single point to output some portion of a holographic image. Guided-mode light that is undiffracted by a surface acoustic wave continues to propagate in the waveguide and is available for diffraction for subsequent surface acoustic waves. This propagating light can be modulated by additional transducers in a cascaded diffractive fashion (see Figure 13). The embedded structure required to produce the flat panel holographic display is the input and output couplers combined with the waveguides. Each output coupler, i.e volume grating, requires a transducer to alter the propagating light and cause a percentage of the light to out couple. Therefore, the following steps in development of this holographic display are the addition of a direct write process for creating metal transducers coupled with the directly written waveguides and input / output couplers.

ACKNOWLEDGEMENTS

This research has been supported by consortium funding at the MIT Media Laboratory, by the Center for Terrestrial Sensing at the MIT Media Laboratory, and by Air Force Research Laboratory contract FA8650-14-C-6571. The authors gratefully acknowledge facility use and technical assistance by the MIT Nanostructures Laboratory, the MIT Scanning Electron-Beam Lithography facility, the MIT Research Laboratory of Electronics, the MIT Center for Bits and Atoms, and the Mazur Group at Harvard University.

REFERENCES

[1] Smalley, D. E., Smithwick, Q., Bove, V. B., Barabas, J. and Jolly, S., "Anisotropic leaky-mode modulator for holographic video displays, *Nature* 498, 313-317 (2013).

[2] Smalley, D. E., Smithwick, Q., Barabas, J., Bove, V. M., Jolly, S. and Della Silva, C., "Holovideo for everyone: a low-cost holovideo monitor," *Proceedings of the 9th International Symposium on Display Holography* (2012).

[3] Gattass, R. R. and Mazur, E. "Femtosecond laser micromachining in transparent materials," *Nature Photonics*, 2(4), 219-225 (2008).

[4] Burghoff, J., Hartung, H., Nolte, S. and Tannermann, A., "Structural properties of femtosecond laser-induced modifications in LiNbO3," *Applied Physics A* 86(2), 165-170 (2007).

[5] He, R., An, Q., Jia, Y., Castillo-Vega, G. R., V. de Aldana, J. R. and Chen, F., "Femtosecond laser micromachining of lithium niobate depressed cladding waveguides," *Optical Materials Express* 3(9), 1378-1384 (2013).

[6] Thomson, R. R., Campbell, S., Blewett, I. J., Kar, A. K. and Reid, D. T., "Optical waveguide fabrication in z-cut lithium niobate (LiNbO3) using femtosecond pulses in the low repetition rate regime," *Applied Physics Letters* 88, 111109 (2006).

[7] Savidis, N., Jolly, S., Datta, B., Karydis, T. and Bove, V. M., "Fabrication of waveguide spatial light modulators via femtosecond laser micromachining," *Proc. SPIE 9759* (2016).

[8] Reichman, W. J., Krol, D. M., Shah, L. , Yishino, F., Arai, A., Eaton, S. and Herma, P., "A spectroscopic comparison of femtosecond-laser-modified fused silica using kilohertz and megahertz laser systems," *Journal of Applied Physics* 99, 123112 (2006).

[9] Ponader, C., Schroeder, J. and Streltsov, A., "Origin of the refractive index increase in laser written waveguides in glasses," *Journal of Applied Physics* 103(5) (2008).

[10] Li, Y. et al, "Holographic fabrication of multiple layers of grating inside soda-lime glass with femtosecond laser pulses," *Applied Physics Letters* 80, 1508-1510 (2002).

[11] Nordin, G. P, Johnson, R. V., and Tanguay, A. R., "Diffraction properties of stratified volume holographic optical elements," *Journal of the Optical Society of America A* 9(12), 2206 (1992).